Oxidation of Metals
https://doi.org/10.1007/s11085-022-10142-2

BRIEF REPORT

Development of a Novel, Impurity-Scavenging, Corrosion-Resistant Coating for Ni-Based Superalloy CMSX-4

M. E. Pek[1] · A. K. Ackerman[1] · M. Appleton[2] · M. P. Ryan[1] · S. Pedrazzini[1]

Received: 22 July 2022 / Revised: 6 December 2022 / Accepted: 9 December 2022

Abstract

Sulfur, a common impurity arising from atmospheric and environmental contamination, is highly corrosive and detrimental to the lifespan of nickel superalloys in jet engines. However, sulfur-scavenging coatings have yet to be explored. Our study presents the successful development of a stable, uniform, impurity-scavenging Ni-Mn coating on Ni-based superalloy CMSX-4, through electroplating. The coating was characterised via combined scanning transmission electron microscopy and energy-dispersive X-ray spectroscopy. An optimal coating thickness of > 600 nm was deposited. The coated alloy was exposed to corrosive salt mixture 98% Na_2SO_4–2% NaCl at 550 °C for 100 h, mimicking engine exposure conditions, thereby proving that the coating successfully trapped sulfur and prevented its diffusion into an underlying alloy. This work presents a promising development for the prevention of sulfur-induced corrosion in industrial setting such as gas turbine engine, where the effects of sulfur diffusion into the bulk alloy could lead to premature failure.

M. E. Pek and A. K. Ackerman have been contributed equally to this work.

✉ S. Pedrazzini
s.pedrazzini@imperial.ac.uk

[1] Department of Materials, Imperial College London, South Kensington Campus, Exhibition Road, London SW7 2AG, UK

[2] Rolls-Royce Plc, PO box 31, Derby DE24 8BJ, UK

Published online: 26 December 2022

Graphical Abstract

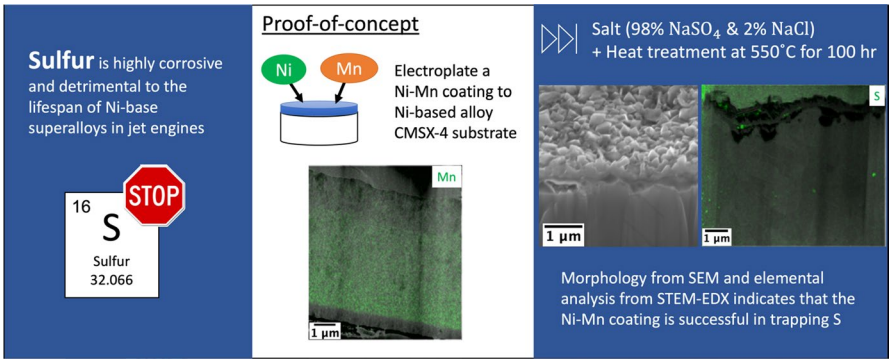

Keywords Nickel alloys · Electroplating · Coating · Corrosion · Scanning/transmission electron microscopy (STEM)

Introduction

Ni-based superalloys are commonly used as high-temperature structural materials for turbine discs and blades in aero-engines and industrial gas turbines [1]. To increase efficiency, the modern gas turbine entry temperature (TET) has steadily increased over the years, and currently exceeds the melting point of the nickel-based alloys that are exposed to it [1]. Such extreme operating conditions have made the protection offered by internal cooling channels and thermal barrier coatings crucial. In recent years, changes in design and airflow resulted in aero-engine turbine blades experiencing more extreme operating temperatures in different stages of flight. Due to local salt deposits from particulate ingestion and atmospheric sulfur ($SO_{2/3}$) exposure from volcanic activity, coupled with fuel exposure and exposure to the exhausts of other aircraft, new corrosion mechanisms have emerged in turbine blades [2, 3]. Metal sulfide formation and sulfur-induced corrosion-fatigue pose a considerable risk, as corrosion by sulfur generally leads to more rapid failure compared to oxygen and other contaminants [4].

Efforts to counteract sulfidation and hot corrosion by alloying have traditionally centred around the use of chromium and aluminium due to their ability to form stable, slow-growing, surface passivating oxide scales [6, 7]. Sulfur also affects oxide scale spallation in nickel-based superalloys, therefore many gettering efforts have been made, since the 1980s–90 s [5]. Elements such as hafnium or zirconium have been added to the alloys to improve creep properties since the 1960s [8] and are presumed to act as sulfur scavengers [9], although they have been shown to have larger affinity for oxygen, in air [10].

Manganese, unlike most metals, possesses similar sulfidation and oxidation rates with similar activation energies (88 kJ mol^{-1} and 81 kJ mol, respectively) [4]. Some

previous studies on the effect of manganese alloying on the oxidation and corrosion resistance of nickel superalloys were performed on turbine disc alloys. Manganese formed a surface layer of spinel $MnCr_2O_4$, which proved to be excellent surface protection in static furnace exposures to air at 700–800 °C [11, 12]. However, systematic studies assessing the behaviour of manganese-containing alloys in sulfur-containing environments at 750 °C (as opposed to studies with only oxygen/air) found this addition to be detrimental to the properties. Manganese is a strong sulfur scavenger, and its presence therefore increased the damage depth through faster sulfur incorporation and the formation of sub-scale MnS sulfides [11]. A relatively small addition of manganese (1 wt%) provided a significant detrimental effect on the damage depth and corrosion resistance of the alloy [11]. The addition of Mn, although proven beneficial to the oxidation resistance of turbine disc alloys, could lead to a deterioration in the creep resistance if added to turbine blades.

Turbine blade alloys are, however, rarely used uncoated. Coatings have the dual purpose of protecting against heat (thermal barrier), as well as conferring corrosion and oxidation resistance [1]. Coatings range from relatively cheap aluminide diffusion barriers all the way to more complex, multi-layer thermal barrier coatings [13]. Historically, many methods have been employed to improve the corrosion resistance of thermal barrier coatings, including smart overlay coating concepts, layered thermal barrier coating structures and diffusion barriers [14, 15]. However, to our knowledge, no studies exist in the open scientific literature exploring the addition of manganese *into a coating*. Based on previous work, it is reasonable to hypothesise that contaminant sulfur would react directly with a manganese coating, minimising the damaging effects of incorporation in the underlying bulk alloy. A manganese-containing coating would be expected to partly oxidise in-service, the same way any other conventionally used aluminide/chromide coating also would. However, sulfidation and oxidation rates are similar and in addition to the benefits of having the sulfur react with the coating rather than the alloy, manganese oxide has also been shown to provide surface passivation on nickel superalloys [12].

The present paper explores a feasibility study of incorporating Mn into an electroplated coating, for enhanced surface protection of nickel-based superalloys for jet engines. This is the first proof of concept aiming at locking the sulfur into the surface to minimise damage to the underlying alloy.

Electroplating Methods

Electrolytic manganese metal is used in a wide range of applications, such as the production of steel and aluminium alloys. Manganese electrodeposition is technically and commercially challenging due to low current efficiency and high cell voltage required to achieve a uniform layer. Manganese electrodeposition from ammonium sulfate and chloride has been most widely studied [16–19]. However, due to the potential safety hazards associated with the toxicity of ammonium salts and the challenges that scaling up to industrial levels of production would present, an alternative route using co-deposition of nickel and manganese was sought [16, 19–21]. Ni-Mn alloy contains enough manganese for an initial proof-of-concept study, to

prove the validity of the hypothesis that sulfur scavengers incorporated into a coating can minimise damage to the underlying alloy. Furthermore, low Mn concentration (< 0.5 wt.%) in both direct current (DC) and pulse plated (PP) Ni-Mn coatings were found to exhibit significant thermal stability, up to 700 °C, as compared to Ni deposits due to its smaller grain structure [22]. The thermal stability makes the coating more effective in gauging whether manganese will improve sulfidation and hot corrosion resistance.

The co-deposition of nickel-manganese (Ni-Mn) from a modified nickel sulfamate plating solution was performed. The method was modified from that reported by Ananth [20], using a different manganese salt (manganese(II) chloride tetrahydrate). All salts were purchased from commercial sources and were used without further purification. The electrolyte consists of 350 g l^{-1} nickel(II) sulfamate tetrahydrate ($Ni(SO_3NIH_2)_2$ $4H_2O$, Fluka, ≥ 98.0%) and 10 g l^{-1} nickel(II) chloride hexahydrate ($NiCl_2$ $6H_2O$ Sigma Aldrich,≥ 95.0%), 35 g l^{-1} boric acid (H_3BO_3, AnalaR, 99.5%) and 10 g l^{-1} manganese(II) chloride tetrahydrate ($MnCl_2$ $4H_20$, Alfa Aesar, 99% metal basis), with grade I deionised water. A three-electrode setup was employed for typical electrodeposition of Ni-Mn coating with a platinum wire as the counter electrode and Ag/AgCl reference electrode (+ 0.197 V SHE), using an Ivium CompactStat.h standard potentiostat.

Initially, pure Ni rods were used to optimise the coating deposition conditions (purchased from Goodfellows, cut into 8.5 mm diameter, 5 mm long discs, and surface finish ground with 4000 grit SiC paper). Then, samples of single-crystal nickel superalloy CMSX-4, supplied by Rolls-Royce plc in the form of 6.5-cm-long, 9.4-mm-diameter cylinders, were used as the working electrode (substrate). These cylinders were cut into 5-mm-long discs and progressively ground on both sides to a 4000 grit SiC paper smooth flat surface finish. Copper tape was placed on one side of the sample, with silver paint applied over it to ensure conductivity, to prepare the discs for electrodeposition. To limit the area exposed to the electrolyte, epoxy was applied around the disc and over the silver paint, exposing only the front surface of the disc.

Coating conditions were optimised on pure polycrystalline Ni discs initially. Linear sweep voltammetry (LSV) was performed for both nickel sulfamate electrolytes with and without the addition of manganese chloride at a sweep rate of 10 mV s^{-1}(Fig. 1). The presence of Mn in the electrolyte led to an additional peak at − 1.47 V (vs Ag/AgCl), comparable to that of Atanassov and Mitreva [21]. This potential corresponds well to the standard reduction potential of Mn^{2+}/Mn couple of − 1.37 V (vs Ag/AgCl).[1] Through a series of trials for a plating duration of 500 s each, − 1.0 V was chosen, as it produced a smooth surface that still contained manganese. The presence of manganese at a lower potential than indicated by the LSV is supported by literature that found that incorporating Mn into Ni films is not a result of the electrochemical reduction but rather a surface reaction at the cathode, which therefore is the limitation of the coating composition [19, 20]. To quality-check the coating, the FIB was used on a − 4.0 mA (− 1.0 V) pure Ni-coated sample, to expose

[1] https://chem.libretexts.org/@go/page/6649.

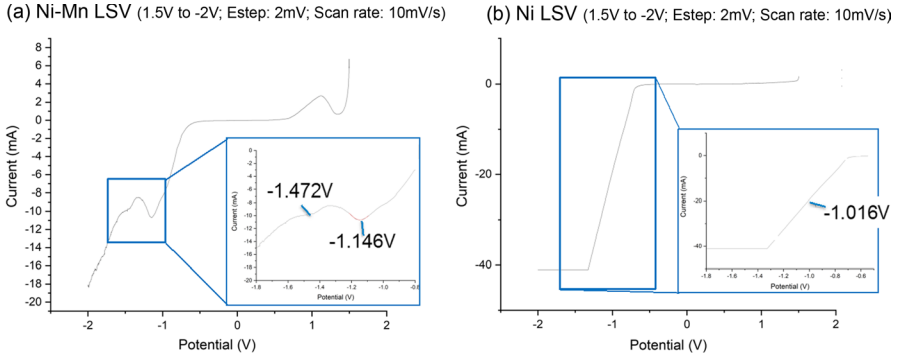

Fig. 1 Linear sweep voltammetry obtained for **a** nickel-manganese-containing electrolyte and **b** nickel-containing electrolyte. Both curves show deposition at around − 1.15 V for nickel, and **a** confirms the potential for the electrodeposition of manganese to be about − 1.47 V

a cross section of the coating, confirming uniformity, adhesion and measuring thickness (with ImageJ), which was found to be an average of 1.48 µm. This value is consistent with predictions obtained from Faraday's second law of electrolysis, which allows the coating thickness to be calculated from the electrochemical charge passed (from the experimental current and duration of the electrodeposition) indicating a high reaction efficiency.

After optimisation of the coating conditions with pure Ni discs, commercially available CMSX-4 nickel-based superalloy discs were cut, ground to 1200 SiC surface finish and then successfully electroplated with the Ni-Mn coating, using the previously optimised procedure. DC electroplating was used, as pulse plated samples were found to contain significantly lower amounts of Mn, as shown by Atanassov and Mitreva [21]. Two CMSX-4 specimens were produced, one to be used as a control sample and one to be used for static corrosion testing. The duration of plating was extended to 3000 s, to allow for a coating thickness of more than 5 µm to be obtained. The coating procedure performed on CMSX-4 samples produced similar deposition rates, thickness and uniformity compared with pure nickel samples, with the exception of a rougher surface finish, which could also be a result of the extended duration of the experiment or due to the increase in external stresses on the sample surface [21].

Characterisation and Corrosion Methods

One coated nickel sample was sprayed with a saturated salt solution containing 98vo l%Na_2SO_4–2vo l%NaCl, on a hot plate held at 200 °C. The final salt mixture concentration on the surface was 9.9 mg cm^{-2}. Two coated CMSX-4 samples (salted and unsalted) were then subjected to a static (no applied load) thermal exposure for 100 h at 550 °C in air. After exposure, the samples were washed with water to remove residual unreacted salt from the surface, then mounted side-on in cold-setting epoxy (Demotec 70). The epoxy was allowed to set overnight before grinding

and polishing using 0.4 µm oxide particle solution (OPS) made of colloidal silica. Some of the salted samples were left un-mounted, attached to an aluminium stub using carbon tape and the free surface was then used for TEM liftout, as per the previously outlined procedure.

A focused ion beam (FIB) microscope (Zeiss Auriga 4524 dual-beam SEM–FIB) was then used to obtain cross-sectional images and higher magnification images with a working distance of 5 mm, operating at a beam voltage of 20 kV. Further images were also obtained at 5 kV for improved surface resolution. The FIB, set at 30 kV and 2 nA, was used to mill a 7-µm-deep trench to allow the cross section of the coating to be imaged. Both salted and unsalted samples were imaged. Site specific liftouts were completed using a Helios DualBeam SEM–FIB fitted with an Omniprobe. Scanning transmission electron microscopy (STEM) was performed using a JEOL 2100F fitted with an Oxford Instruments energy-dispersive X-ray (EDX) detector at 200 keV. When peak overlaps presented issues, other higher peaks were used to correctly identify the location of specific elements (e.g. Mo-Kα was used instead of Mo-Lα for accurate sulfur identification).

Results

SEM analysis of pre-heat-treated discs at − 1.0 V revealed that the increased electroplating duration of 500 s resulted in significantly lower amounts of Mn (~ 0.4 at.%) available in the coating, which is likely to be a result of the depletion of Mn ions in the electrolyte. As a result, two further changes were made to the initially proposed method. Firstly, the electrolyte was refreshed every 500 s to ensure a high amount of manganese. However, peeling started occurring after ~ 1500 s. The higher manganese content of ~ 1.8 at%, measured by EDX, could have resulted in higher residual stresses [19, 22], which resulted in lower adhesion. Secondly, twice the original manganese chloride concentration was added to the electrolyte, which increased the manganese content in the coating without altering the surface finish.

The Ni-Mn coating produced at − 1.0 V at twice the manganese concentration was examined with TEM (Fig. 2) to determine the coating morphology and composition. The coating was found to be uniform, adherent, nanocrystalline and Mn rich, although the EDX map showed a decrease in manganese content with distance away from the substrate: the highest concentration is closer to the CMSX-4 substrate, then as the Mn in the plating solution is consumed up by the deposition process, less Mn is deposited as the coating grows, therefore the outer surface contains a lower concentration of Mn. Further optimisation of the plating conditions including replenishing the electrolyte more often could provide more uniformity but for a first proof of concept could be performed on the resultant, adherent, Mn-enriched coating. The sample from Fig. 2 was therefore salted and corroded following the outlined procedure.

Angular protrusions formed on the salted sample surface, which were absent in the unsalted specimen. The unsalted specimen preserved the morphology of the coating after the heat treatment, as shown by SEM in Fig. 3a, b. A cross section of the salted sample obtained by ion milling is shown in Fig. 3c. The coating

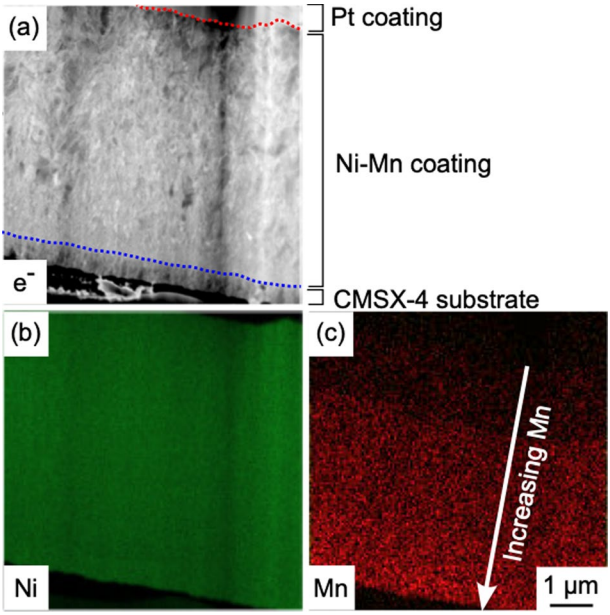

Fig. 2 Ni-Mn coating on CMSX-4. **a** HAADF-STEM image showing cross section of Ni-Mn coating on CMSX-4. Corresponding STEM-EDX of **b** Ni and **c** Mn showing the distribution of Mn in the Ni-Mn coating

thickness was found to be 611 nm, significantly lower than what is expected from Faraday's second law of electrolysis, suggesting some delamination, spallation or vaporisation has occurred. Volatile oxide and metal species could have formed at the metal-coating interface, which could have induced partial mechanical flaking of the oxide layer. Thermodynamically, the coating could be expected to form nickel and manganese oxides, chlorides or sulfides, none of which are volatile at the temperature of interest. However, several of the chlorides that could have formed from the underlying CMSX-4 alloy are volatile ($FeCl_3$—$T_m = 307$ °C, $AlCl_3$—$T_m = 108$ °C, $TiCl_4$—$T_m = -24$ °C) and could have contributed to thinning of the coating by scale spallation, flaking or volatilisation.

The angular protrusions now observed on the coating of the salted sample (Fig. 3b, c) are typical of sulfide formation [23, 24]. Post-heat treatment STEM-EDX proved the presence of a manganese coating on the surface of the nickel-base alloy and confirmed that the coating successfully trapped sulfur after salt exposure (Fig. 4). STEM-EDX also showed areas of increased O concentration, indicating the formation of MnO after heat treatment. As our heat treatments were performed in air, with low-level sulfur additions, the correlation between Mn–O is stronger than the correlation between Mn-S, which is due to a higher amount of oxide forming, compared to sulfides. The tests were performed by exposing the Mn-containing coating to both oxygen and sulfur in an attempt to simulate jet engine working conditions as closely as possible.

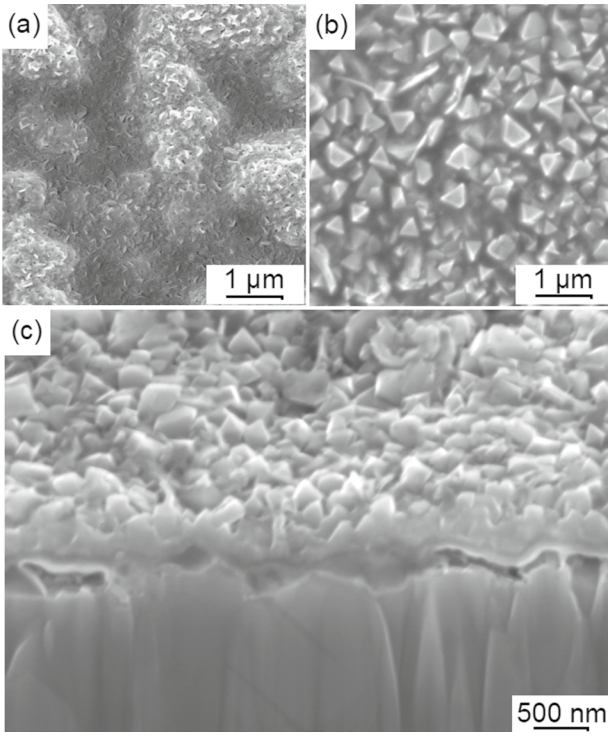

Fig. 3 Comparison of surface morphology post-heat treatment at 550 °C for 100 h. **a** CMSX-4 Ni-Mn coated, unsalted sample after heat treatment at 550 °C for 100 h **b** CMSX-4 Ni-Mn coated, salted after heat treatment at 550 °C for 100 h, and **c** FIB cross section of (**b**) showing salt layer and Mn coating, with CMSX-4 bulk material

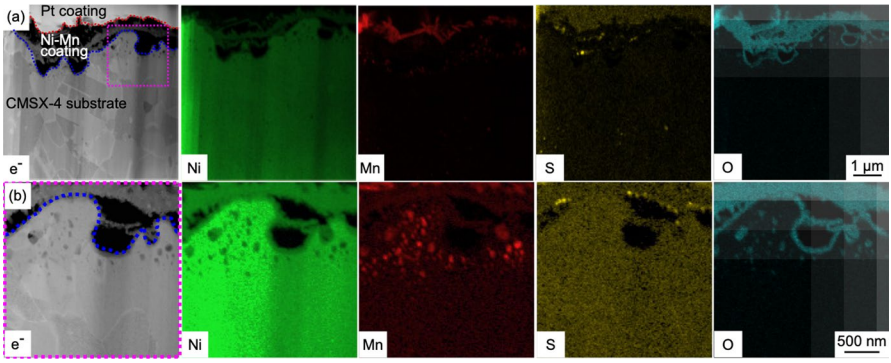

Fig. 4 HAADF-STEM image of CMSX-4 salted and heat-treated at 550 °C for 100 h. Corresponding STEM-EDX of Ni, Mn, S and O, showing the Ni alloy substrate, Ni-Mn coating, oxide layer and sulfur trapped within the Ni-Mn coating, with **a** showing an overview, and **b** and increased magnification of the highlighted area

Having said that, no evidence of sulfur penetration in the underlying alloy was found, therefore the proposed coating successfully trapped the sulfur on the surface.

Some sub-surface microstructural evolution is also observed in Fig. 4, with most notably the formation of these MnO particles. Disconnected oxide particles such as these have been long suspected of being a source of fatigue crack initiation, therefore further quasi-static and dynamic tests will have to be performed to assess the viability of the coating and optimise its performance. However, previous studies in which nickel-based superalloys containing Mn are exposed to sulfur with no coating have shown that the sulfide formation generally occurs at lower depth than oxide formation [11]. Preventing the sulfur ingress would therefore be minimising the damage depth, despite the sub-surface oxide formation.

Conclusions

In conclusion, in this first proof-of-concept study, discs of Ni-based superalloy CMSX-4 were successfully electroplated with a Ni-Mn coating. The Ni-Mn electrodeposition condition was optimised, and − 1.0 V for 3000 s gave the best thickness, uniformity and adhesion of the coating. However, further systematic studies or wider parametric conditions could improve uniformity of composition.

Results from exposure to a corrosive salt mixture 98% Na_2SO_4 and 2% NaCl in laboratory furnaces at 550 °C showed sulfur trapped in the surface above the coating, preventing damage to the bulk alloy. This is extremely promising, and it is thought to be due to the formation of manganese sulfides.

This is a first proof-of-concept study; therefore, further studies are required to optimise the testing different corrosive compounds, including gaseous $SO_{2/3}$, as well as different coating techniques and conditions, particularly in light of the fact an-impurity-scavenging coating would get "used-up" during service. Although large volumes of air go through a jet engine, the sulfur content is both highly detrimental and relatively low (ppm). The low sulfur content gives some credit to the notion of disposable coatings being adequate for impurity-scavenging purposes.

Although more work is required to establish, among other things, how long the coating would last in-service (our tests were performed for 100 h, engine time would require the coating to last in excess of 15,000 h) and/or possibly the requirement and frequency of reapplication of the coating, our current findings are an extremely promising development for future incorporation of sulfur scavengers into corrosion-resistant coatings.

Author Contributions ME Pek and AK Ackerman did the experimental work and wrote the manuscript's first draft. MP Ryan, M Appleton and S Pedrazzini co-supervised the work, gave feedback and edited the draft.

Funding This work is co-funded by Rolls-Royce plc and the Engineering and Physical Sciences Research Council (EP/S013881/1). The Royal Academy of Engineering is gratefully acknowledged for in-kind support in the form of an Associate Research Fellowship. MPR acknowledges support from the Armourers and Brasiers company. Data contained in this manuscript will be made available upon reasonable request to the authors.

Declarations

Conflict of interest The authors declare no conflict of interest.

References

1. R. C. Reed, *The Superalloys: Fundamentals and Applications*. Cambridge University Press; 2006. doi:https://doi.org/10.1017/CBO9780511541285.
2. L. Brooking, S. Gray, K. Dawson, et al., Analysis of combined static load and low temperature hot corrosion induced cracking in CMSX-4 at 550 °C. *Corrosion Science* **163**, 2020 (108293).
3. E. Kistler, W. Chen, G. H. Meier, and B. Gleeson, A new solid-state mode of hot corrosion at temperatures below 700 °C. *Materials and Corrosion* **70**, 2019 (1346–1359).
4. D. J. Young, *High temperature oxidation and corrosion of metals*, (Elsevier, Amsterdam, 2008).
5. S. Floreen and R. H. Kane, Effects of environment on high-temperature fatigue crack growth in a superalloy. *MTA*. **10**, 1979 (1745–1751).
6. C. S. Giggins and F. S. Pettit, Oxidation of Ni-Cr-Al Alloys Between 1000° and 1200°C. *Journal of The Electrochemical Society* **118**, 1971 (1782).
7. M. C. Stasik, F. S. Pettit, G. H. Meier, A. Ashary, and J. L. Smialek, Effects of reactive element additions and sulfur removal on the oxidation behavior of fecral alloys. *Scripta Metallurgica et Materialia* **31**, 1994 (1645–1650).
8. R. F. Decker and J. W. Freeman, The mechanism of beneficial effects of boron and zirconium on creep properties of a complex heat-resistant alloy. *Transactions of the AIME* **218**, 1960 (277–285).
9. Y.-R. Zheng, Y.-L. Cai, Z.-C. Ruan, and S.-W. Ma, Investigation of effect mechanism of hafnium and zirconium in high temperature materials. *Hangkong Cailiao Xuebao/Journal of Aeronautical Materials* **26**, 2006 (25–34).
10. S. Pedrazzini, D. J. Child, T. Aarholt, et al., On the effect of environmental exposure on dwell fatigue performance of a fine-grained nickel-based superalloy. *Metall and Mat Trans A* **49**, 2018 (3908–3922).
11. E. Anzini, N. Glaenzer, P. M. Mignanelli, M. C. Hardy, H. J. Stone, and S. Pedrazzini, The effect of manganese and silicon additions on the corrosion resistance of a polycrystalline nickel-based superalloy. *Corrosion Science* **176**, 2020 (109042).
12. S. Pedrazzini, D. J. Child, G. West, et al., Oxidation behaviour of a next generation polycrystalline Mn containing Ni-based superalloy. *Scripta Materialia* **113**, 2016 (51–54).
13. J. R. Nicholls, Advances in coating design for high-performance gas Turbines. *MRS Bull.* **28**, 2003 (659–670).
14. J. R. Nicholls, Designing oxidation-resistant coatings. *JOM.* **52**, 2000 (28–35).
15. J. R. Nicholls, N. J. Simms, W. Y. Chan, and H. E. Evans, Smart overlay coatings—concept and practice. *Surface and Coatings Technology.* **149**, 2002 (236–244).
16. O. Aaboubi, A.-Y. Ali-Omar, E. Dzoyem, J. Marthe, and M. Boudifa, Ni–Mn based alloys as versatile catalyst for different electrochemical reactions. *Journal of Power Sources.* **269**, 2014 (597–607).
17. A. J. Gibson, B. Johannessen, Y. Beyad, J. Allen, and S. W. Donne, Dynamic electrodeposition of manganese dioxide: temporal variation in the electrodeposition mechanism. *Journal of The Electrochemical Society* **163**, 2016 (H305–H312).

18. W. Li and S. Zhang, In situ ellipsometric study of electrodeposition of manganese films on copper. *Applied Surface Science* **257**, 2011 (3275–3280).
19. J. Lu, D. Dreisinger, and T. Glück, Manganese electrodeposition—A literature review. *Hydrometallurgy* **141**, 2014 (105–116).
20. M. V. Ananth, Corrosion studies on electrodeposited Nickel-Manganese coatings. *Transactions of the IMF* **75**, 1997 (224–227).
21. N. Atanassov and V. Mitreva, Electrodeposition and properties of nickel-manganese layers. *Surface and Coatings Technology.* **78**, 1996 (144–149).
22. S. H. Goods, J. J. Kelly, and N. Y. C. Yang, Electrodeposited nickel ?Manganese: an alloy for microsystem applications. *Microsystem Technologies* **10**, 2004 (498–505).
23. E. A. Marquis, A. A. Talin, J. J. Kelly, S. H. Goods, and J. R. Michael, Effects of current density on the structure of Ni and Ni–Mn electrodeposits. *Journal of Applied Electrochemistry* **36**, 2006 (669–676).
24. A. A. Talin, E. A. Marquis, S. H. Goods, J. J. Kelly, and M. K. Miller, Thermal stability of Ni–Mn electrodeposits. *Acta Materialia* **54**, 2006 (1935–1947).